Astron. Astrophys. 281, 348–354 (1994)

ASTRONOMY AND ASTROPHYSICS

Properties of UCM 2303+1702, a new seyfert 2 galaxy*

M. Rego[1], J. Zamorano[1], J. Gallego[1], and A. Vitores[1,2]

[1] Departamento de Astrofísica, Facultad CC Fisicas, Universidad Complutense, E-28040 Madrid, Spain
[2] EUIT Industrial, Universidad Politécnica, E-28012 Madrid, Spain

Received December 7, 1992; accepted June 20, 1993

Abstract. The galaxy UCM 2303 + 1702, not previously known, was identified during the Universidad Complutense de Madrid (UCM) objective-prism survey. The optical spectrum displays emission lines with a blueward asymmetry. Forbidden lines cover a wide range of ionization exhibiting full width at half maximum (FWHM) unusually broad. An analysis of ionization range and the emission line ratios measured in the spectrum leads to a Seyfert 2 classification. The contour map of isophotes of the CCD image shows an Sbc–Sc^+ spiral, nearly face-on, in disagreement with previous works reporting an anticorrelation between the [O III] line width and the Hubble morphological type in Seyfert parent galaxies. High quality IRAS coadded data have been used to study the far-infrared properties.

Key words: galaxies: individual: UCM 2303 + 1702 – galaxies: Seyfert

1. Introduction

We are carrying out a long term project with the main purposes of finding and analyzing low metallicity galaxies. We have started by surveying fields using a low resolution objective-prism and working in the Hα region. A significant number of star-forming galaxies are missed by optical surveys in the blue because of their low-excitation spectra. This is why objective-prism surveys in Hα are a powerful method to identify that sort of galaxies. The efficiency of this observational procedure was corroborated in the Northern and Southern Hemisphere by the results obtained by Kinman (1983), Wamsteker et al. (1985), Rego et al. (1989, 1993) and Zamorano et al. (1989, 1992).

The survey is being performed at the German–Spanish Observatory (Calar Alto, Almería). Every objective-prism plate was visually scanned through a binocular microscope at low magnification (10 ×) by three observers. Each candidate is classified according to the Hα intensity, strength of the continuum and appearance on the Palomar Observatory Sky Survey (POSS) prints.

Although a large fraction of the galaxies identified are star-forming objects, there are some of them that when analyzed from higher resolution spectroscopic data, show evidence of activity. This is the case of UCM 2303 + 1702 [RA(1950) = $23^h03^m27.0^s$, DEC(1950) = 17°02′06″], which is studied here from CCD images and moderate resolution spectroscopy acquired with 2.2 and 3.5 m telescopes at the German–Spanish Observatory respectively. On the basis of these observations some general properties and the excitation mechanisms are derived. Complementary information is also raised from the far-infrared fluxes resulting of coadding the original IRAS scans. These data when analyzed jointly with the Seyfert radio luminosities compiled from the literature, allow us to estimate the 1415 MHz luminosity of UCM 2303 + 1702. These results are briefly discussed in the context of the existence of a radio lobe structure.

2. Observations and reductions

2.1. Spectrophotometry

The spectrum of UCM 2303 + 1702 was obtained in November 1989 with the twin spectrograph attached to the Cassegrain focus of the 3.5 m telescope at Calar-Alto Observatory. A slit of width 2.35″ was placed centered in the nucleus with PA = 90°, i.e. in the E–W direction. The spectrograph has two channels which allow simultaneous observations of the blue and red spectra. In the first we used an RCA CCD detector with equivalent pixel size of 30 μm, together with a 300 gr mm^{-1} grating, which provide a dispersion of 144 Å mm^{-1} (4.3 Å pixel^{-1}). Although the wavelength coverage is larger we could use only the range λλ4000–5500 Å, due to the low efficiency of the RCA chip in the violet region. A GEC CCD detector with pixel size of 22 μm and a 400 gr mm^{-1} grating was used for the red side leading to a linear dispersion of 108 Å mm^{-1} (1.84 Å pixel^{-1}). The available spectral range is from λλ5950 to 7000 Å. The exposure time was 3600 s in both colors. The spatial scale was 0.8 and 1 arcsec/pixel in the blue and red channels respectively. We aimed to obtain spectra with sufficiently good signal-to-noise ratios to

Send offprint requests to: M. Rego
* Based on observations taken at Calar Alto German-Spanish Observatory (Almería, Spain)

be able to recognize and measure emission lines with intensities only a few per cent of the strong [O III] and Hα lines. The standard star, EG 247, was repeatedly observed at different air masses in order to monitor the atmospheric extinction and ensure suitable flux calibration. Reduction of the data was carried out using the ESO image-processing system software package (MIDAS), and involves flat-fielding, wavelength calibration, sky subtraction, extinction correction and conversion to absolute fluxes. Both spectra were measured for redshift using the stronger emission lines. The instrumental profile FWHM as measured in the comparison arc spectra and in the night sky lines is 8.1 Å (480 km s^{-1}) in the blue side and 6.3 Å (280 km s^{-1}) in the red one.

2.2. Direct images

CCD images of UCM 2303 + 1702 were acquired with the 2.2 m telescope of Calar Alto German–Spanish Observatory (Almería, Spain). A RCA CCD chip of 640 × 1024 pixels was used binned on both axis to a final pixel size of 30 μm which is equivalent to 0.35″ on the sky. Images were taken through a Gunn–Thuan r filter on December 1988, September 1990 and December 1990 with exposure times of 900, 1800 and 1800 s respectively. The point spread function of seeing for all the images as determined from the measurements of unsaturated stars on each frame is 1.5″ (FWHM). Atmospheric conditions were photometric only during the December 1990 run. Absolute calibration was obtained by observing repeatedly during the night a set of standard stars, taken from the list given by Kent (1985a). High S/N ratio dome flats and exposures of the sky taken in twilight were also obtained. The standard procedure of bias removal, dark current subtraction and flat fielding using both dome and sky flat-fields was performed with the MIDAS.

2.3. Near-infrared photometry

The observations were made with the 1.5 m Carlos Sánchez infrared Telescope (TCS) at the Izaña Observatory (Tenerife). The CVF InSb photometer was used with a 15″ aperture. The beam throw was 45″ east–west, larger than the optical radius as measured in the CCD images. The object was centered visually at the maximum brightness at the TV screen. The galaxy was observed in the Johnson J (1.25 μm), H (1.65 μm), and K (2.2 μm) broad band filters. Reduction was performed by observing the stars HR 8905, HR 660, HR 508, and HR 1140 several times during the night. The uncertainties resulting from the weakness of the object and repeated observations, each one consisting of consecutive integrations, represent the dominant source of error in the final magnitudes.

2.4. IRAS data

The IRAS flux densities were derived by coadding the original IRAS scan data at the Infrared Processing and Analysis Center (Rutherford Appleton Laboratory, Oxford, England). Since UCM 2303 + 1702 is a point source as seen by IRAS, the data was coadded in one-dimensional sense only. These fluxes measured in Janskys are $F(12\ \mu m) = 0.05L$, $F(25\ \mu m) = 0.10$:, $F(60\ \mu m) = 0.38$ and $F(100\ \mu m) = 0.66$. In agreement with the PSC Catalogue (Lonsdale et al. 1989), the colon denotes a moderate quality flux density and L an upper limit.

3. Results

3.1. Optical and near-infrared properties

In Fig. 1, the spatial distribution of the spectrum along the slit is shown. The spectrum displayed in Fig. 2 is the result of adding all the spatial scans with significant signal, i.e. 22″, by using the optimal extraction algorithm proposed by Horne (1986) and implemented within MIDAS. This spectrum shows strong [N II] lines with a high degree of ionization typical of an AGN. Detailed profiles for Hβ and Hα spectral regions are shown in Fig. 3a and b respectively. The line fluxes were measured using a two-degree polynomial fit to the local continuum on either side of the line and integrating the continuum subtracted flux over the line profile. The accuracy of the line fluxes measurements is affected by the underlying absorption, blending of the lines and fitting of the local continuum. The interstellar reddening was corrected using the reddening function of Whitford (1958) as normalized and tabulated by Kaler (1976). The intrinsic Hα/Hβ ratio was taken 3.10 (Veilleux & Osterbrock

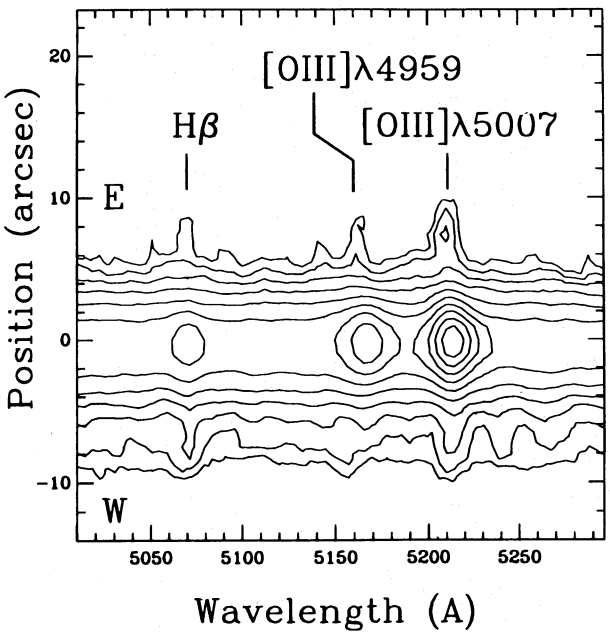

Fig. 1. Contour plot of the two-dimensional spectrum, showing the extended emission in the Hβ and [O III]λλ4959, 5007 Å lines. The intensity scale is logarithmic with the lowest contour representing 20 net counts/pixel

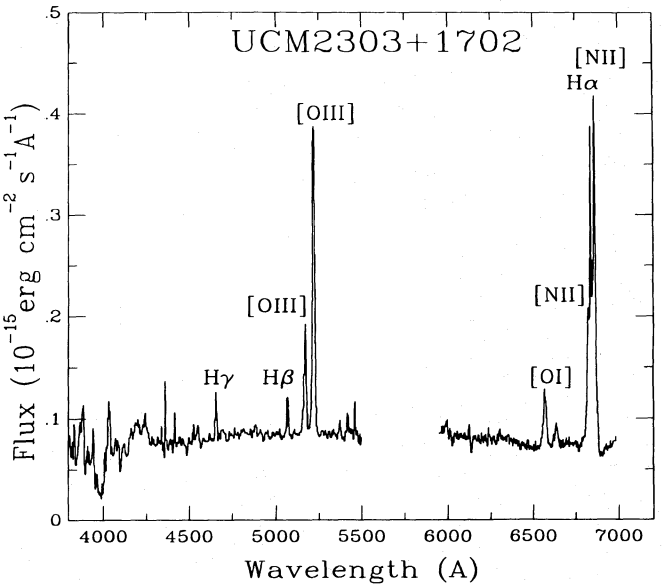

Fig. 2. Composite of the red and blue scans of UCM 2303 + 1702 taken with the twin spectrograph at the Cassegrain focus of the 3.5 m telescope at Calar-Alto German–Spanish Observatory

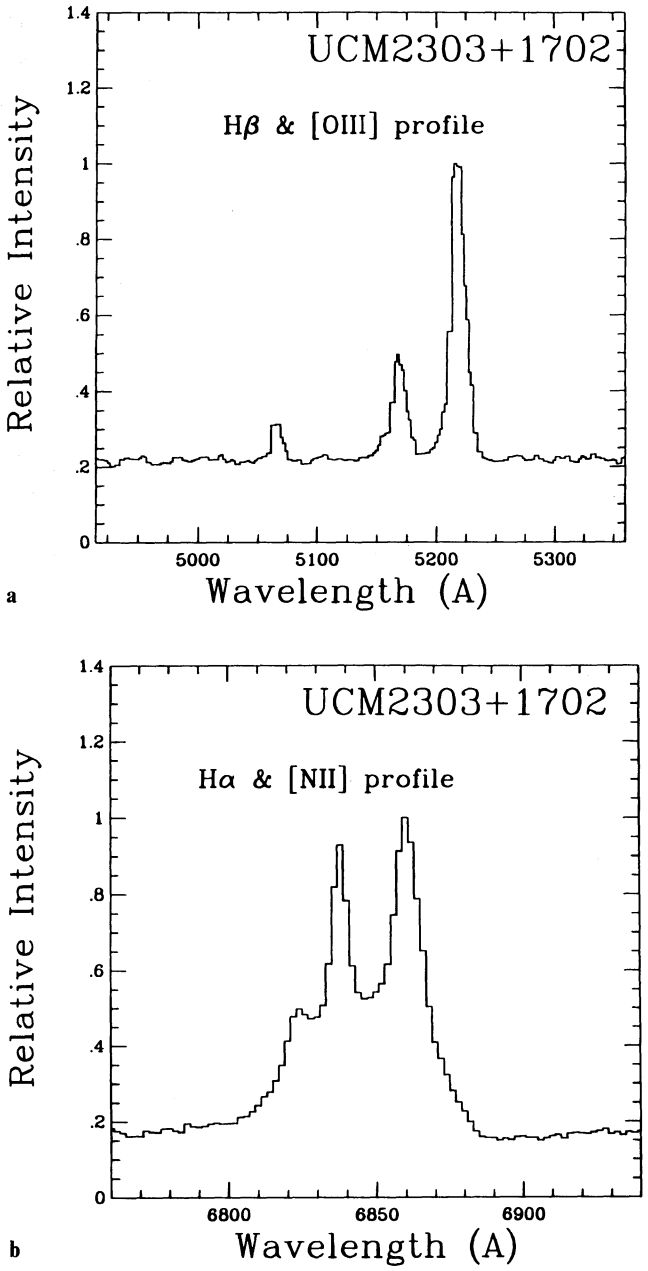

Fig. 3a and b. Detailed profiles: **a** Hβ and [O III] lines, **b** Hα and [N II] lines

1987), although the activity class is not known a priori, but the difference in the reddening correction is very small among the Seyfert types. It was possible to measure the strengths and equivalent widths of additional narrow emission lines. The redshift was computed as a weighted mean considering the shift of all measurable emission-lines in the spectrum, using their equivalent widths as relative weight. In this way a value of $z = 0.0420 \pm 0.0001$ was obtained. The FWHMs were measured by fitting Gaussians to the profiles, or blending lines such Hα, [N II]$\lambda\lambda$6548, 6563, and [S II]$\lambda\lambda$6716, 6731. The comparison lines, observed on the same night with the same instrumental settings, were assumed to be intrinsically much narrower than the instrumental profile, and thus to define the instrumental FWHM. The identified lines and their intensities are listed in Table 1.

An examination of Table 1 and a detailed inspection of the spectrum reveals the following points: (1) The strong lines display a blueward asymmetry as can be seen in Fig. 3a (2) A wide range of ionization stages arising lines as [Fe VI] and [Fe VII] lines together with others representing low stages of ionization such as [O I] and [S II] are found. The most likely explanation for these lines is that the gas is photoionized by a nonthermal source, which produces a large amount of high-energy ionizing photons. However, since the [O I]λ6300/[O I]λ6363 ratio measured in the spectrum is very similar to the theoretical ratio, 3/1, this implies that [Fe X]λ6375 has a weak contribution to the [O I]λ6363, [Fe X]λ6375 blend and ionization is not high enough to classify UCM 2303 + 1702 as Seyfert 1. (3) The Fe II lines are completely blended and were identified on the basis of the comparison of UCM 2303 + 1702 spectrum with sharper-line objects observed in higher resolution. No attempt was made to deblend the Fe II lines. An upper limit value of 0.1 10^{-15} erg cm^{-2} s^{-1} (1σ above rms of noise in the adjacent spectral region) was derived for the sum of the Fe II multiplets 37 and 38. The strength of this feature has been shown to be correlated with the total strength of all multiplets of optical Fe II emission. In fact Collin-Souffrin et al. (1986) find that Fe II λ4570, mainly multiplets 37 and 38, accounts for about 25% of the total Fe II emission. There are large uncertainty in measurement of the Fe II strength and any comparative study suffers from the lack of clear definition as well as personal bias. (4) The spectrum exhibits also

Table 1. The UCM 2303 + 1702 emission line fluxes relatives to $F(H\beta) = 100$

Ion	λ (Å)	F_{obs}	F_{cor}	EW (Å)
[O II]	3727	273	462	−23
[Ne II]	3777	55	148	−5
[Ne III]	3869	150	235	−11
[Fe V]	4071	64	91	−4
H γ[b]	4340	19	24	−1
[O III]	4363	38	47	−2
[Fe III][a]	4658	5	6	−0.3
He II[b]	4686	20	21	−1
Hβ	4861	100	100	−6
[O III]	4959	361	350	−21
[O III]	5007	1012	963	−58
[Fe VII]	5159	43	39	−3
[N I][a]	5199	2	3	−0.2
He I[b]	5875	19	14	−1
[Fe VII][b]	6087	17	11	−1
[O I]	6300	257	160	−18
[O I]	6363	104	63	−7
[N II]	6548	497	286	−37
Hα	6563	542	310	−40
[N II]	6583	1417	803	−108

Notes
$F(H\beta) = 0.49\ 10^{-15}$ erg cm^{-2} s^{-1}.
$F(H\beta)_c = 3.18\ 10^{-15}$erg cm^{-2} s^{-1}.
[a] At 1σ level.
[b] At 2σ level.

absorption line characteristics of integrated late-type stars.

Excitation conditions in the narrow emission-line regions of UCM 2303 + 1702 can be studied by applying the specific spectral criteria recommended by Veilleux & Osterbrock (1987). The optical line ratio diagram of $\lambda5007/H\beta$ vs. [O I]$\lambda6300/H\alpha$ is the best single tool to classify emission-line objects according to the dominant ionizing–heating mechanism. In particular, AGNs are distinguished from SBNs by their larger values of [O I] $\lambda6300/H\alpha$. But it is very useful also to use [O III] $\lambda5007/H\beta$ against another reddening-insensitive line ratio, [N II]$\lambda6583/H\alpha$.

When the above line ratios of UCM 2303 + 1702 are plotted at the diagnostic line ratio diagrams (Fig. 4), the position of the object is clearly within the boundaries of the Seyfert 2 region. It can be noted a small shift to the right part of the both diagrams. In the first, the shift could be due to the low dispersion of the spectrum and the errors intrinsic to the deblending procedure of Hα and [N II] lines. For the second diagram, it can be caused by the uncertainty due to the weakness of [O I]$\lambda6300$ line.

However to be classified as Seyfert 2, UCM 2303 + 1702 should fulfill the condition established by the own definition of Seyfert 2: spectra do not have very broad permitted lines (which characterize Seyfert 1s), but instead have permitted lines widths similar to forbidden lines widths (Shuder & Osterbrock 1981). This criterion, considered a necessary but not sufficient condition for the Seyfert phenomenon, is violated only by a few Seyfert 2s. UCM 2303 + 1702, like Mk 622 (Whittle 1992; MacKenty 1990), presents a [O III]$\lambda5007$ FWHM larger than the Balmer lines.

UCM 2303 + 1702 indeed has anomalous broad forbidden lines. Early analysis found Seyfert galaxies to have systematically broader lines than Starburst galaxies, and [O III]$\lambda5007$ FWHM > 300 km s^{-1} was suggested as a defining characteristic (Shuder & Osterbrock 1981). The improvement of the resolution and the observation of fainter sources, settle the [O III] FWHM active nuclei median in 350 km s^{-1} (40% of the objects show values below 300 km s^{-1}), which is considerably less than previously thought (Whittle 1985). Larger values are actually anomalous in fact only 4 galaxies present [O III]$\lambda5007$ FWHM > 700 km s^{-1} in the list collected by Whittle (1992), which included 140 Seyfert 2 and Seyfert 1 galaxies. Between them can be found NGC 1068, that was initially considered as a Seyfert 2 prototype. The FWHM values of these galaxies and UCM 2303 + 1702 are given in Table 2. Their dispersion velocities are far to high to be originated from a normal galaxy velocity field, and also very different of the 350 km s^{-1} median.

In order to study off-nuclear emission, the long-slit spectrum of UCM 2303 + 1702 was analysed. Several of

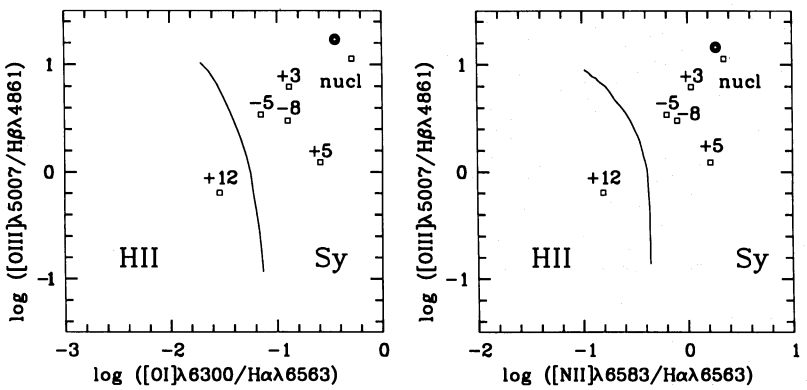

Fig. 4. Emission-lines intensity ratios. Solid curve is from Veilleux & Osterbrock (1987). A circle denotes the integrated spectrum. Squares represent the radial behavior of emission-line gas in the galaxy using the diagrams. Numbers are distances from the nucleus expressed in arcseconds

Table 2. Seyfert 2 galaxies with anomalous [O III] FWHM

Galaxy	FWHM (km s^{-1})		
	[O III]	Hα	Hβ
Mk 3	958	950	908
Mk 78	1075	710	563
Mk 273	700		
Mk 622	1160	350	350
NGC 1068	1060		
UCM 2303 + 1702	803 ± 30	617 ± 31	530 ± 23

the emission lines of interest showed signal-to-noise ratios allowing a reasonable measurement of line intensity out to 12″ from the nucleus in both directions along the slit. At this location spiral structure starts to become prominent. As the object appears to be nearly face-on, velocity differences are very small and no attempt was made to remove velocity shifts due to galaxy rotation. Line fluxes were measured at each row after binning at the same spatial scale both spectra (1″).

We have examined the radial behavior of emission-line gas in the galaxy using the Veilleux & Osterbrock (1987) diagrams drawn from the above reference. These diagrams are shown in Fig. 4. Characteristic locations of H II regions and Seyfert galaxies on these figures are delimited by a solid line in the central part of each diagram. Observed ratios are plotted for points ranging from 0″ to 12″ in both directions from the nucleus. The line–ratio diagrams show a consistent radial trend in both cases in the sense that ratios in the nucleus are typical of Seyfert galaxies and become more characteristic of H II regions when moving away from the nucleus.

In consistence with the above results, the derived $J - K$ color index obtained for UCM 2303 + 1702, 1.31 ± 0.36, is typical of a Seyfert galaxy.

A deep CCD r image was built by means of stacking the three individual frames. The resulting image, scaled to the December 1990 values, is displayed in Fig. 5. UCM 2303 + 1702 appears as a spiral galaxy, nearly face-on. The integrated magnitude is $r = 16.19 \pm 0.09$. With the help of the program GASP (Davis et al. 1985), ellipses were fitted to the isophotes. The brightness profile is plotted in Fig. 6 where the solid line represents the best fit obtained by the summation of a bulge $r^{1/4}$ law (de Vaucouleurs 1948) and an exponential disk law (Freeman 1970).

In order to analyse the parameters produced by the bulge–disk decomposition, some relations between them and the morphological type have been examined. So, the central surface brightness $\mu_0 = 19.80$ in the disk points to a spiral type classification using the μ_0 versus Hubble type I diagram of Kent (1985b). In the same way, this galaxy presents an exponential scale length of the disk $\log h = 0.30$, but in the μ_0 versus $\log h$ diagram by Kent (1985b) the segregation between S and SO systems is not very clear. Regarding to the bulge parameters, UCM 2303 + 1702 presents an effective bulge surface brightness $\mu_e = 25.23$, a very low value corresponding to a very late-type spiral galaxy. Moreover, the effective radius r_e corresponding to this μ_e, result to be $r_e = 5.6''$, $\log r_e = 0.75$; this pair of values ($\log r_e$, μ_e) places UCM 2303 + 1702 at the Sbc–Sc$^+$ region in the Kent (1985b) diagram. Another important parameter results to be the bulge/disk ratio expressed by the form of the ratio of bulge to total luminosity (B/T). For

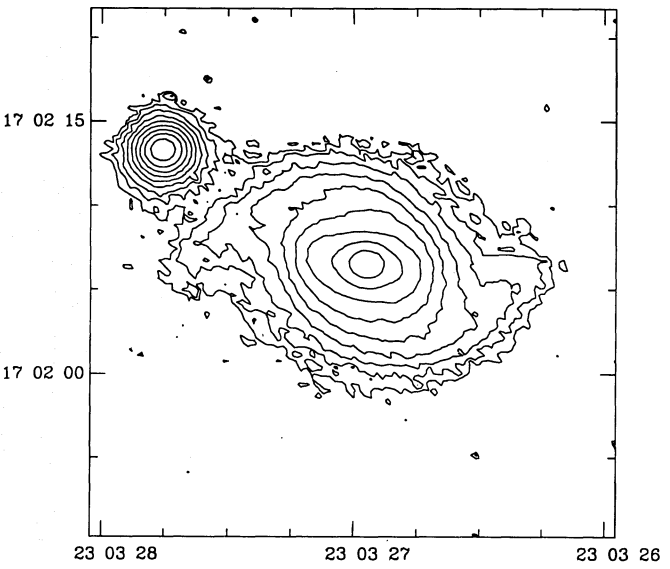

Fig. 5. Contour map of isophotes of UCM 2303 + 1702. Magnitude interval in steps of 0.5 mag arcsec^{-2}. The faintest isophote represents 24 mag arcsec^{-2}. North is up and east to the left

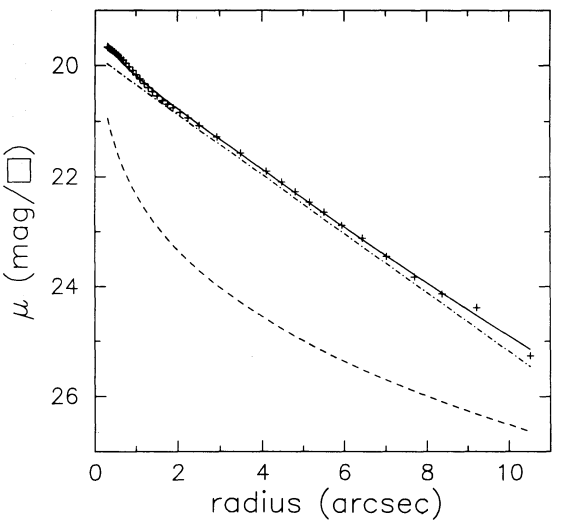

Fig. 6. Brightness profile of UCM 2303 + 1702 in the Gunn–Thuan r band. The solid line represents the best fit obtained by the summation of a bulge $r^{1/4}$ law (dashed line) and an exponential disk law (dash-dotted line)

UCM 2303 + 1702 we have derived a B/T = 0.13, a value corresponding to an Sbc type by Simien & de Vaucouleurs (1986) and Sbc–Sc$^+$ type by Kent (1985b).

According to Kent (1985b), there are some methods to avoid the problem of the characterization of the light distribution by parameters which depend on the way to obtain the light profile. One of these methods consists in the concentration parameter defined as $c = 5\log[r(0.8)/r(0.2)]$ where $r(0.2)$ and $r(0.8)$ are the radii which contain 20% and 80% of the total luminosity of the galaxy, respectively. For UCM 2303 + 1702 we have obtained $c = 3.38$, a typical value for a Sbc–Sc$^+$ morphological type. Finally, our B/T = 0.13 assigns an Sc$^+$ type in Table 4 of Kent (1985b) which lists the median values of B/T for spirals of different morphological types, although this should be taken only as indicative due to the uncertainty of this classifications. In summary, the profile appears clearly dominated by a disk component corresponding to a very late-type spiral galaxy. This result is an additional evidence of the anomaly of the UCM 2303 + 1702 in the sense that early morphological types exhibit [O III] profiles broader than those observed in the later types (Veilleux 1991).

3.2. Far-infrared properties

The origin of far-infrared (FIR) emission from active galactic nuclei has long been controversial. The main mechanisms responsible for FIR emission are non-thermal emissions from a nucleus and thermal emission from dust. The relative importance of these processes appears to vary in the AGN class due to the large diversity in their 10–100 μm energy distributions. From far and near infrared and r colors we compute $\log \nu f_\nu$ which are represented against the frequency in Fig. 7. The energy distribution places UCM 2303 + 1702 among the objects having IR fluxes dominated by the external regions outside the compact nucleus, where the stellar contamination becomes significant in the optical and near infrared (Ward et al. 1987).

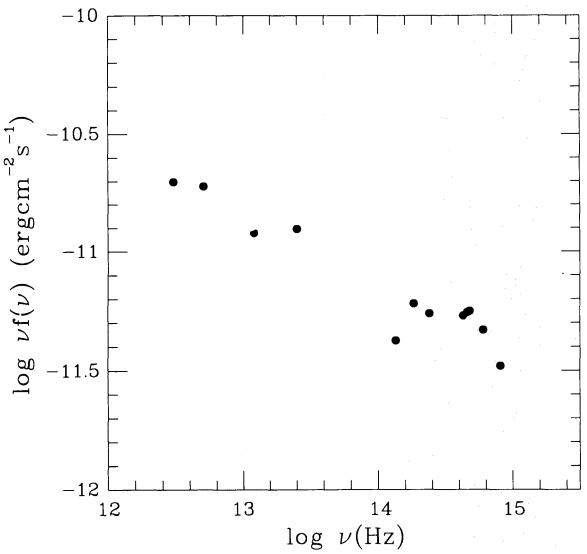

Fig. 7. Energy distribution of UCM 2303 + 1702 between 0.65 and 100 μm

More information about the behavior of UCM 2303 + 1702 in the FIR can be drawn from the $\alpha(25,60)$ vs. log[O I]λ6300/Hα and FIR luminosity diagrams elaborated by Mouri & Taniguchi (1992). In the first, UCM 2303 + 1702 appears between the power law model and the best fits of starburst nuclei data. In the second, it is placed above the spiral normal galaxies region. One plausible explanation is that the spectrum of UCM 2303 + 1702 involves a nuclear and starburst components, hence far-IR emission can be considered as a mixture of the flat component from a nonthermal source and the steep component from dust heated by young stars, with a likely contribution from the interstellar radiation field (the disk component) powered by an evolved stellar population.

4. Conclusions

UCM 2303 + 1702 presents a Seyfert 2 nucleus hosted in a Sbc–Sc$^+$ spiral galaxy nearly face on with a peculiar broadening of the forbidden lines. Radial trends seen in the optical emission-line diagrams for UCM 2303 + 1702 (Fig. 4) can easily be explained qualitatively in terms of photoionization by a Seyfert nucleus and by hot stars. This result is also confirmed by the IRAS FIR observations.

Why UCM 2303 + 1702 has broader [O III] emission lines and the majority of Seyfert do not, is an interesting question. Ulvestad and Wilson (1984) have showed from a statistical study, that Seyfert 2s appear more luminous than type 1's in the radio region. Furthermore relations between radio emission and several features observed in Seyfert 2 galaxies have been pointed out: a correlation has been noticed between 1415 MHz and the infrared and the [O III]λ5007 luminosities; the blueward asymmetry of stronger forbidden lines, appears also in large sample of active nuclei having powerful steep-spectrum radio sources, etc. This result can be interpreted as assuming that the forbidden lines observed in the UCM 2303 + 1702 are emitted by a gas which is accelerated by two mechanisms; one, gravitational, which is responsible of the [O III] broadening observed in Seyferts with nonlinear radio morphologies; another one, caused by the central engine, which is characteristic of the radio linear sources, leading the emitting gas to higher velocities. So we can conclude that radio observations would be a desirable addition to the data for this galaxy.

Acknowledgements. This work was supported in part by the Spanish "Programa Sectorial de Promoción General del Conocimiento" under Grant No. PB89-124.

References

Collin-Souffrin S., Dumont S., Joly M., Peguinot D., 1986, A&A 205, 19

Davis L.E., Cawson M., Davies R.L., Illingworth G., 1985, AJ 90, 169
de Vaucouleurs G., 1948, Annales d'Astrophysique 11, 247
Freeman K., 1970, ApJ 160, 811
Horne K., 1986, PASP 98, 609
Kaler J.B., 1976, ApJS 31, 517
Kent S.M., 1985a, PASP 97, 165
Kent S.M., 1985b, ApJS 59, 115
Kinman T.D., 1983, MNRAS 202, 53
Lonsdale C.J., Helou G., Good J.C., Rice W., 1989, Catalogued Galaxies and Quasars in the IRAS Survey, Jet Propulsion Laboratory, Pasadena
MacKenty J.W., 1990, ApJS 72, 231
Mouri H., Taniguchi Y., 1992, ApJ 386, 68
Rego M., Zamorano J., González-Riestra R., 1989, A&AS 79, 443
Rego M., Cordero M., Zamorano J., Gallego J., 1993, AJ 105 (in press)
Shuder J.M., Osterbrock D.E., 1981, ApJ 250, 55
Simien F., de Vaucouleurs G., 1986, ApJ 302, 564
Ulvestad J.S., Wilson A.S., 1984a, ApJ 278, 544
Ulvestad J.S., Wilson A.S., 1984b, ApJ 285, 439
Veilleux S., 1991, ApJS 75, 383
Veilleux S., Osterbrock D., 1987, ApJS 63, 295
Wamsteker W., Prieto A., Vitores A., et al., 1985, A&AS 62, 255
Ward M., Carleton N., Elvis G., Fabbiano G., Willner S., et al., 1987. in: Khachikian E., Fricke K., Melnick (eds.) Observational Evidence of Activity in Galaxies, IAU Symp. 121. Reidel, Dordrecht, p. 119
Whitford A.E., 1958, AJ 63, 201
Whittle M., 1985, MNRAS 213, 1
Whittle M., 1992, ApJ 79, 49
Zamorano J., Rego M., González-Riestra R., Rodríguez R., 1989, Ap&SS 170, 353
Zamorano J., Gallego J., Rego M., Vitores A.G., González-Riestra R., 1992, AJ 104, 1000